Supporting Information

Strain Modulation of Graphene by Nanoscale Substrate Curvatures: a Molecular View

*Yingjie Zhang[1,2,3], Mohammad Heiranian[1,4], Blanka Janicek[5], Zoe Budrikis[6], Stefano Zapperi[6,7,8,9], Pinshane Y. Huang[5], Harley T. Johnson[4], Narayana R. Aluru[1,4], Joseph W. Lyding[1,2], Nadya Mason[3]**

[1]Beckman Institute for Advanced Science and Technology, University of Illinois, Urbana, IL 61801, USA

[2]Department of Electrical and Computer Engineering, University of Illinois, Urbana, IL 61801 USA

[3]Department of Physics and Frederick Seitz Materials Research Laboratory, University of Illinois, Urbana, IL 61801, USA

[4]Department of Mechanical Science and Engineering, University of Illinois, Urbana, IL 61801, USA

[5]Department of Materials Science and Engineering, University of Illinois, Urbana, IL 61801, USA

[6]ISI Foundation, Via Chisola 5, 10126 Torino, Italy

[7]Center for Complexity and Biosystems, Department of Physics, University of Milano, via Celoria 16, 20133 Milano Italy

[8]CNR - Consiglio Nazionale delle Ricerche, Istituto di Chimica della Materia Condensata e di Tecnologie per l'Energia, Via R. Cozzi 53, 20125 Milano Italy

[9]Department of Applied Physics, Aalto University, P.O. Box 11100, Aalto, FI-00076 Espoo, Finland

*Email: nadya@illinois.edu

1. Nanosphere assembly

SiO_2 nanospheres were purchased from nanoComposix. Product numbers are SISN20, SISN50, SISN100, and SISN200 for the 20 nm, 50 nm, 100 nm, and 200 nm spheres, respectively. The NSs are dispersed in water, with a concentration of 5 – 10 mg/mL. The NS surface is free of ligands, and terminated with hydroxyl groups, the same species that exist on normal SiO_2 thin film surfaces in air.[1] 300 nm SiO_2 / Si substrates were cleaned via sonication in acetone and IPA, and oxygen plasma, following which SiO_2 NSs were spin-coated. The samples were then baked at 170 °C for 20 minutes on a hotplate to remove the residual water. The NSs form close packed monolayer regions with a size ranging from a few microns to a few tens of microns (which tends to be larger for larger spheres). A large area scanning electron microscopy (SEM) image of the 20 nm NSs, shown in Figure S1, reveals micron-scale monolayer regions and flat regions nearby. For the four NS monolayer systems with varied sizes, high-resolution SEM images all show polycrystalline hexagonal close packing structures (Figure S2), where each single crystalline domain consists of 10s to 100s of nanospheres.

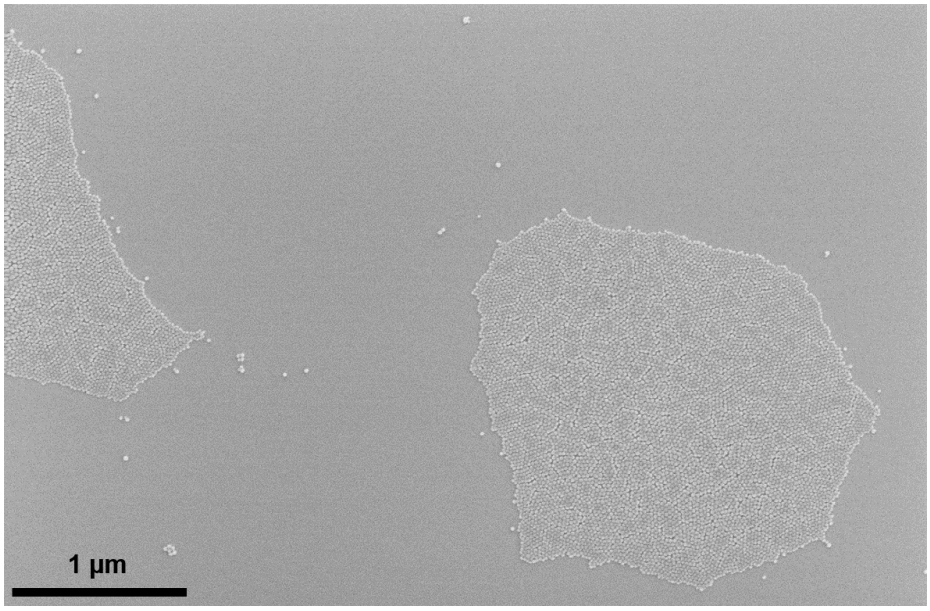

Figure S1. A large-area SEM image of 20 nm SiO_2 NS monolayer. We can see two micron-scale monolayer regions with polycrystalline hexagonal close packed structure. Between the monolayer regions the surface is mostly flat, where single particle or few-particle clusters are sparsely distributed.

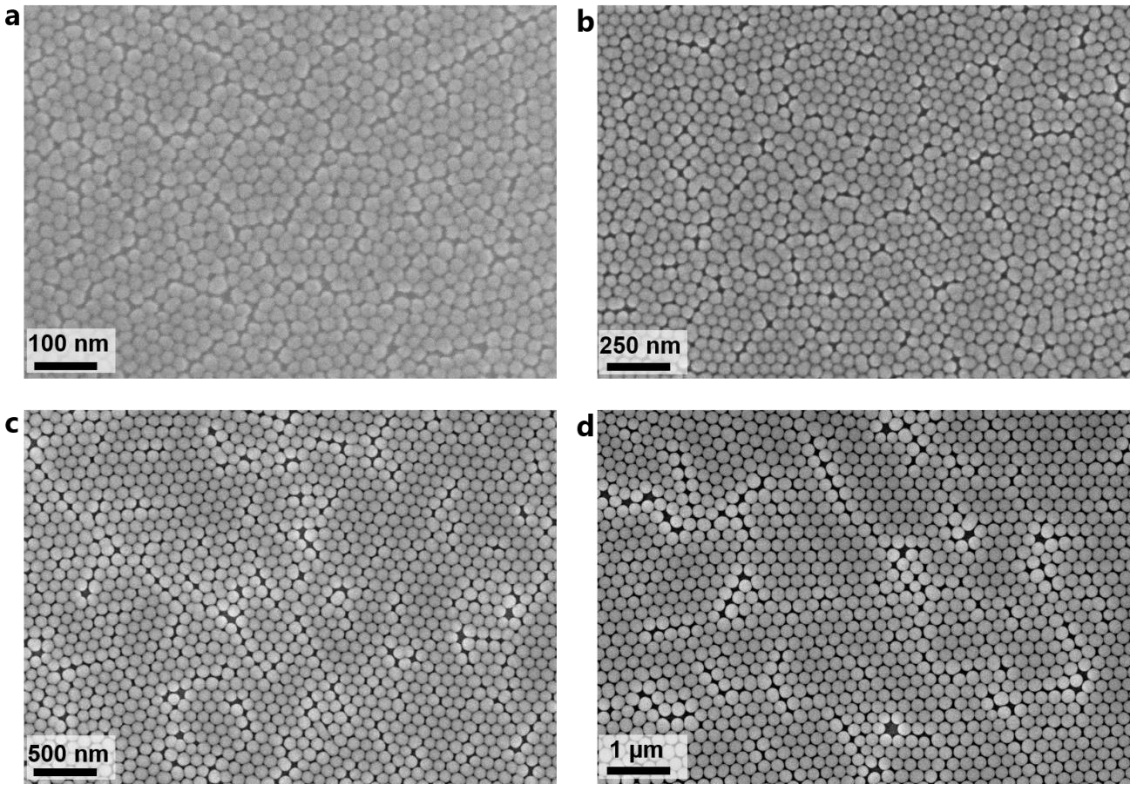

Figure S2. High-resolution SEM images of the SiO_2 nanosphere monolayers. (a, b, c, d) corresponds to NSs with diameter 20 nm, 50 nm, 100 nm, 200 nm, respectively.

2. Graphene transfer

CVD Graphene grown on copper foil was purchased from ACS Material, LLC, and was transferred to the NS substrates using a standard wet transfer technique.[2] Briefly, PMMA was spin-coated to one side of the graphene/copper substrate, dried in air, and the other side (also covered by graphene) was etched using oxygen plasma. The PMMA/graphene/copper stack was placed on ammonium persulfate solution (0.1 M) to etch away the copper. After copper is completely etched away, the ammonium persulfate solution was exchanged with DI water a few times. NS coated substrates were cleaned by oxygen plasma, and used to scoop out PMMA/graphene from water. The PMMA/graphene/NS samples were put in acetone for 1 hour to remove the PMMA, rinsed in IPA, and dried in a critical point dryer.

Atomic force microscopy (AFM) was performed using an Asylum Cypher AFM; the AFM tips were obtained from BudgetSensors with model number Tap150-G. For high-resolution STEM imaging, we fabricated a cross-sectional lift-out sample from the Gr-20 system using an FEI Helios NanoLab 600i dual-beam focused ion beam system. STEM imaging was carried out with a JEOL 2200FS spherical aberration corrected STEM operated at 200 kV, with a 25.6 mrad convergence angle.

3. Raman spectroscopy and strain analysis

3.1 Experimental setup

Confocal Raman spectroscopy was performed at room temperature, in ambient conditions, using Nanophoton Raman 11. Excitation wavelength is 532 nm, and power is 0.5 – 1 mW. 100 × objective was used. All the spectra were fine calibrated using the reference emission lines of a neon lamp.

3.2 Peak position correlation analysis

Spatially averaged areal strain and doping can be extracted from correlation maps of 2D peak position (ω_{2D}) and G peak position (ω_G). As shown in Figure 2c and Figure S3a, with (ω_G^0, ω_{2D}^0) = (1581.6, 2676.9) as the starting point, we can draw a vector to each point (ω_G, ω_{2D}); this vector can be decomposed to the strain axis (green line) and doping axis (cyan line). A downward (upward) projected vector along the strain line (length: l_S) corresponds to tensile (compressive) strain, while along the doping line the vector (length: l_D) is projected towards the right, whether the doping is n- or p-type. Following the analysis in Refs. 3,4, the strain ε (in %) and doping n (in 10^{12} cm^{-2}) can be obtained as:

$$\varepsilon = \frac{l_S}{56.8} = 0.02(\omega_G - \omega_G^0) - 0.028(\omega_{2D} - \omega_{2D}^0), \quad (1)$$

$$n = \frac{l_D}{1.75} = 1.03(\omega_G - \omega_G^0) - 0.47(\omega_{2D} - \omega_{2D}^0). \quad (2)$$

Equations (1) (2) are used to calculate the average areal strain shown in Figure 2d, and average doping in Figure S3b. A positive value of ε corresponds to tensile strain, while doping is assumed to be p-type (it is well known that SiO_2 gives rise to p-type doping in graphene). Here we assumed that the strain is uniaxial, the same assumption used in Refs. 4,5. The actual strain profile can be a combination of uniaxial and biaxial strain due to the geometric frustration of a flat membrane on top of spherical substrates.[6,7] Despite this uncertainty in the strain directions, the strain magnitude estimation from Raman analysis is not significantly affected, since the strain we extract is the areal strain – the change of area, not the length along any particular direction.

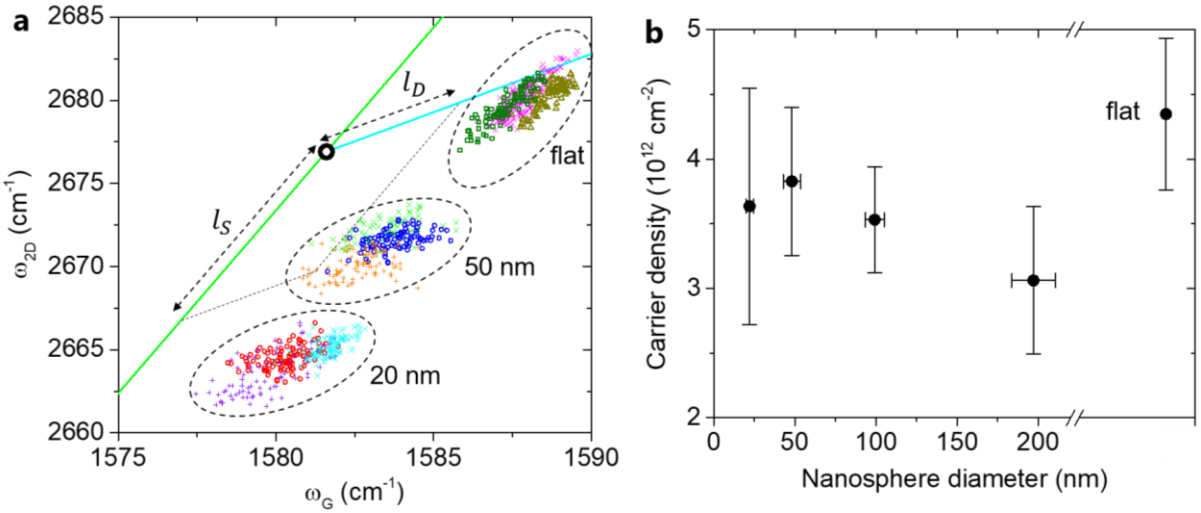

Figure S3. (a) Correlation map of (ω_G, ω_{2D}) for different batches of samples. For each system (flat Gr, Gr-50, Gr-20, marked in dashed ovals), three sets of data were obtained from different samples, and represented with different symbols. Dashed lines represent the vector decomposition process, and l_S and l_D represents the length of the vector projected on the strain

and doping axes, respectively. (b) Doping density as a function of NS size, extracted from the (ω_G, ω_{2D}) correlation analysis. The flat Gr system is also shown for comparison.

Figure S3a shows the (ω_G, ω_{2D}) correlation map for different batches of samples for Gr-20, Gr-50, and flat Gr systems. Although variations in (ω_G, ω_{2D}) exist for different areas on each sample, and different batches of samples for each NS size, the overall strain fluctuation is small enough to allow quantitative comparison of strain among Gr-NS systems having different NS sizes (see Figure 2d). In contrast, doping density of the systems with different NS sizes do not show obvious differences in the presence of large doping variations (fluctuations in carrier density) (Figure S3b). Note that the surface adsorbed oxygen and water molecules on graphene can also contribute to the extracted doping density, since the Raman measurements were performed in ambient conditions.

3.3 Peak width analysis

Besides the peak positions analysis, we also examined the width of the G and 2D peaks Γ_G and Γ_{2D}. It is known that the line width of graphene's Raman peaks depends on a few factors, such as the average doping, average strain, and nanoscale strain variations.[4,5,8,9] Specifically, the G mode is very sensitive to doping, and a lower carrier concentration leads to significant broadening of the G peak due to electron-phonon interactions. Meanwhile, a larger absolute strain magnitude and a higher nanoscale strain variation can both broaden G and 2D peaks.

Figure S4 shows Γ_G and Γ_{2D} as a function of the NS diameter. While Γ_G does not show a clear size-dependence, all the Gr-NS systems have much larger Γ_G than the flat Gr. Since the doping density is similar for all the Gr-NS and flat Gr systems (Figure S3b), and average strain magnitude shows a clear decaying trend as a function of NS size (Figure 2d), neither of these two factors explains the trend shown in Figure S4a. The third possibility, as we mentioned, is the nanoscale strain variations. Since the graphene on NSs experiences periodic height modulation and deformations (Figure 1), the local strain can exhibit large variations, as confirmed by our MD simulations (Figure 4f-h). In comparison, we expect the flat Gr to be mostly smooth and exhibit much smaller strain variations. For Gr-NS systems having different NS diameter, our simulations show similar levels of spatial variation in strain (though the strain gradient is different due to the difference in size scale) (Figure 4f-h). If Γ_G is dominantly determined by the nanoscale strain variations, we expect Γ_G to be similar for Gr-NS with different NS size, and smaller for flat Gr compared to Gr-NS. This agrees with the trend shown in Figure S4a.

While the size dependence of Γ_G seems complicated and indicates the presence of nanoscale strain variations, Γ_{2D} shows a straightforward decaying trend vs nanosphere diameter (Figure S4b), similar to that of ω_{2D} (Figure 2c). This indicates that the average strain magnitude, instead of the local strain variations, may be playing a dominant role in Γ_{2D} modulations.

Caution should be noted that the line width of graphene's Raman modes is always complicated by multiple factors. To more accurately measure the local strain distribution, we would need to perform direct atomic-resolution imaging, such as scanning tunneling microscopy, which is beyond the scope of this paper.

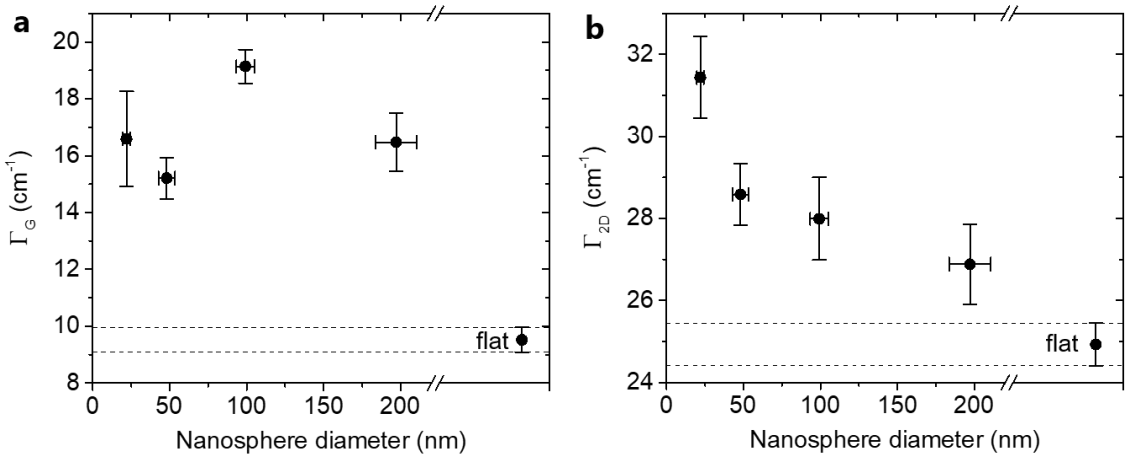

Figure S4. (a) and (b) show the G and 2D Raman peak width respectively, for the Gr-NS systems as a function of nanosphere diameter. The peak width of the flat graphene system is also plotted for comparison.

3.4 Raman map of peak position and peak width

Besides the peak position maps shown in Figure 2b, we present more peak position and width maps on two different Gr-20 samples (Figure S5), each covering both areas of Gr on spheres and Gr on flat SiO_2 substrate. These results consistently show smaller ω_G and ω_{2D}, and larger Γ_G and Γ_{2D}, when comparing Gr-20 with flat Gr, in agreement with the results in Figure 2, Figure S3, and Figure S4.

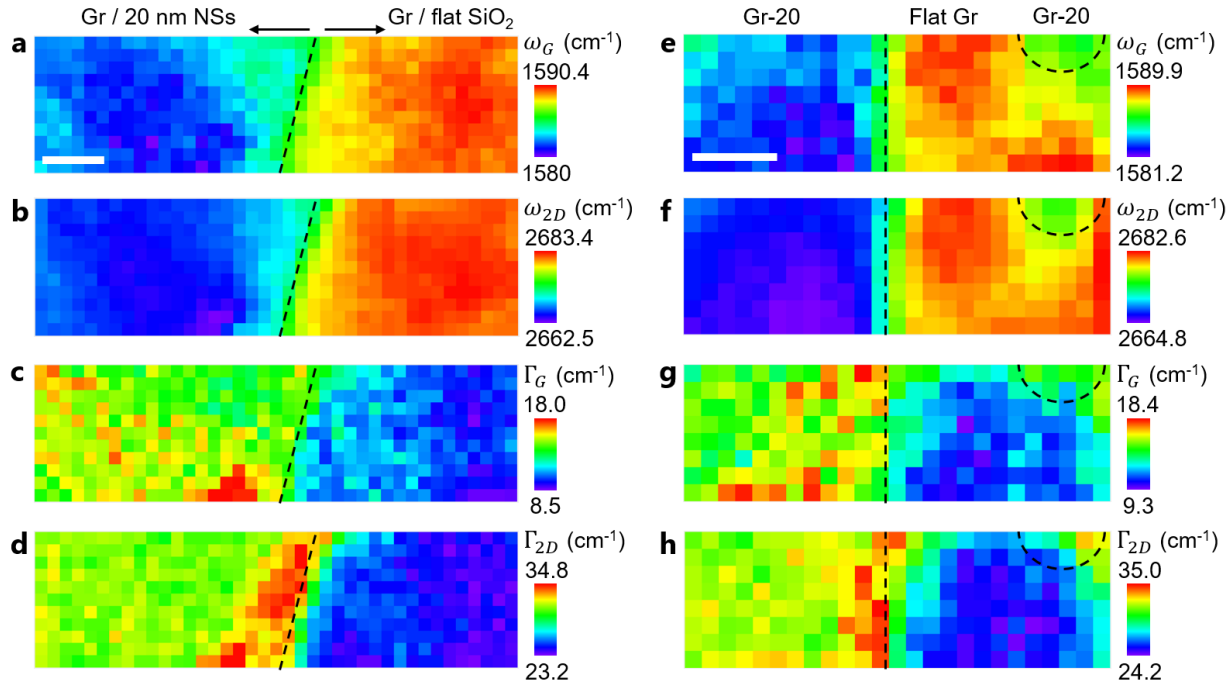

Figure S5. (a-d) ω_G, ω_{2D}, Γ_G, Γ_{2D} maps of a sample containing two regions: Gr / 20 nm NSs on the left, and Gr / flat SiO_2 on the right. The four maps correspond to the same region. (a) and (b) are the same as those in Figure 2b. Scale bar: 1 μm. (e-h) ω_G, ω_{2D}, Γ_G, Γ_{2D} maps of another

sample containing three regions: Gr / 20 nm NSs on the left and at the top right corner, and Gr / flat SiO_2 in the remaining areas. Scale bar: 1 μm.

4. Computational methods

Molecular Dynamics simulations (MD) are performed using the LAMMPS package.[10] Each simulation box consists of a single-layer graphene sheet and a cluster of seven identical SiO_2 nanospheres packed hexagonally together as shown in Figure 4a. The SiO_2 NSs are chosen to have amorphous structure. The graphene sheet and NSs are generated by the Visual Molecular Dynamics (VMD).[11] Four systems with different nanosphere diameters (5 nm, 10 nm, 20 nm and 30 nm) are simulated. The corresponding four graphene sheets, in order from smallest to largest clusters, have dimensions of 14 nm × 14 nm, 27 nm × 27 nm, 52 nm × 52 nm and 81 nm × 81 nm. To model carbon-carbon interactions, the Tersoff potential with the Lindsay-Broido correction is employed, which has been shown to predict mechanical properties that are consistent with experimental results.[12] The non-bonded interactions between atoms of graphene and SiO_2 are modeled by the Lennard-Jones (L-J) potential. The L-J parameters are given in Ref 13. The L-J cutoff distance is 15 Å. The interactions between atoms of SiO_2 are turned off since they are fixed in space in experimental conditions.

Before the simulations, the energy of each system is pre-minimized for 10,000 steps. Each simulation is then performed in NPT (constant pressure, constant temperature) ensemble for 10 ns at a pressure of 1 atm. Temperature is maintained at 300 K by using the Nosè-Hoover thermostat with a time constant of 0.1 ps.[14,15] By monitoring the potential energy, interaction energies, and atomic positions of the system, we find that the initial energy relaxation of the system takes ~5 ps. No significant change in structure and energy occurs during the 5 ps – 30 ps window, which is well before the bending and adhesion of graphene on the NSs. We take the 15 ps configuration as the strain-free structure, which is used as a reference to track the subsequent area change of Gr and calculate the evolution of areal strain. Equilibrium configurations are reached after ~2 ns. No external force is applied in the simulations. Trajectories of graphene atoms are dumped to output files every picosecond. The last 2 ns of the trajectories (10 ns in total) are used for post-processing to extract parameters in the equilibrium state.

5. Additional simulation results

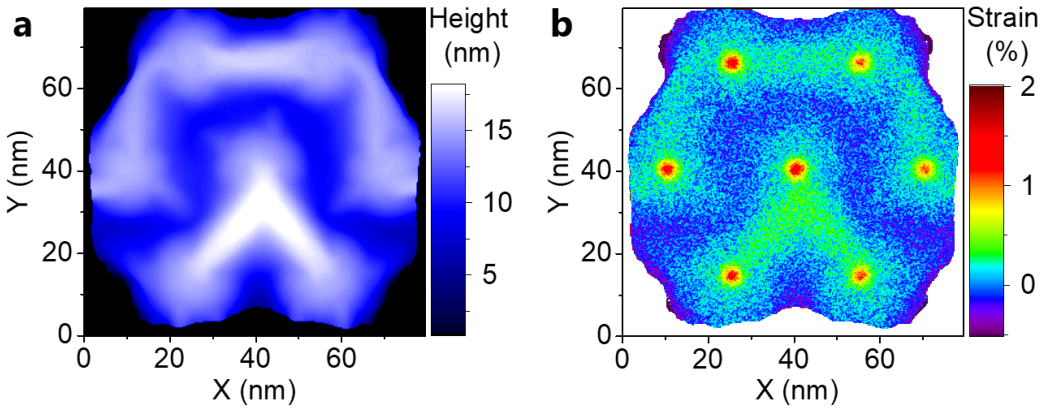

Figure S6. MD simulation results for Gr on 30 nm NSs. (a) Height profile. (b) Strain

distribution.

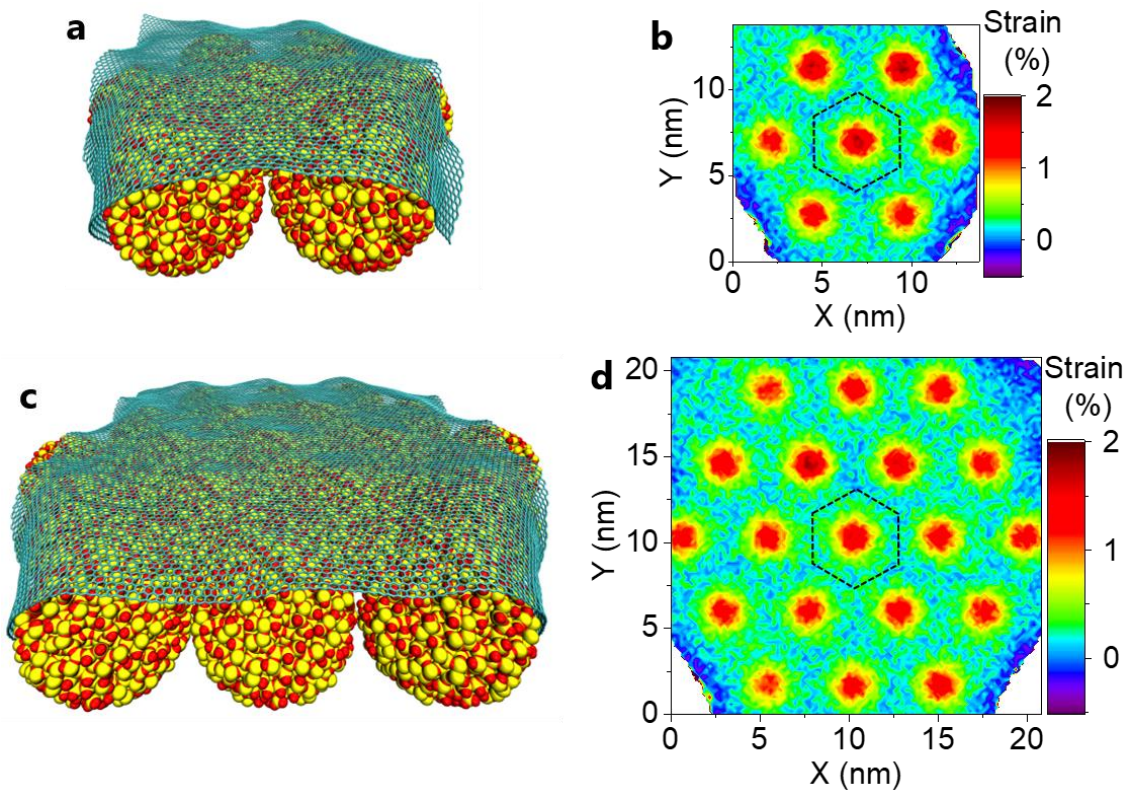

Figure S7. MD simulation results of Gr / 5 nm NS systems with different numbers of spheres. (a) and (b) are the 3D configuration and strain distribution map of Gr on an array of 7 NSs. (b) is identical to Figure 4f. (c) and (d) are the 3D configuration and strain distribution map of Gr on an array of 19 NSs. The central hexagons in (b) and (d) mark the region where average areal strain is calculated, and the results are 1.0002% and 1.0251%, respectively (shown in Figure 4b). We conclude that both the strain distribution and average values are not affected by the limited number of NSs in the MD simulations, and boundary effects are negligible in regions away from the edge.

6. Comparison with prior work on graphene/nanoparticle systems

Previously Gr-SiO_2 nanoparticle hybrids have been demonstrated in two types of systems: 1) Gr on isolated nanoparticles on flat substrates;[16] 2) Gr on few-layer nanoparticle films with random packing structures.[17,18]

Ref. 16 observed wrinkle formation between neighboring nanoparticles separated with large distances on substrates, and thoroughly explained this wrinkle phenomenon in terms of the energy balance between stretching energy, bending energy, and Gr-substrate adhesion energy. However, the adhesion energy was assumed constant for the adhered areas, which, according to our analysis, is insufficient in explaining the curvature-dependent strain modulation mechanisms. Ref. 16 did not measure the magnitude of strain and the size dependence.

Refs. 17,18 reported friction and deformation studies of Gr on multilayer nanoparticle films. Here we note that the top layer of particles in their systems consist of randomly spaced nanoparticles, different from our close-packed monolayer structures. Ref. 17 also performed Raman spectroscopy measurements, and extracted strain values of graphene from the 2D peak shift (G peak was not taken into account). This may not be an accurate estimate considering that the 2D peak position is sensitive to both strain and doping modulations.[3–5] We used the method by Ref. 4 to combine the G and 2D peaks to separate the doping and strain effects (see Section 3.2), and averaged over multiple samples and multiple areas for each sphere size to obtain the statistically significant plot in Fig. 2d. Ref. 17 reported a decrease in 2D peak position as the particle size becomes smaller, which is possibly due to strain enhancements provided that doping effects are independent of particle size. If this is the case, the results will be complementary to ours and demonstrate that this size dependence is in general true for disordered systems too. No molecular level force inhomogeneity mechanisms (involving L-J interactions and scaling of the interaction forces) were proposed in Refs. 17,18.

"Partial adhesion" effects and wrinkle features are observed in Refs. 17,18, although the microscopic structural evolution (at the single sphere level) is not clear, when different nanosphere sizes were chosen. Wrinkle features, observed only in some of the samples in Refs. 17,18, occur mostly near edges of the graphene flakes. In contrast, our samples show wrinkles everywhere in the graphene film (for spheres equal to or larger than 50 nm), and we observe a clear trend of evolution as we tune the size of our nanospheres (Figure 1 in the main text). The edge effects found in Refs. 17,18 may have similar mechanisms as observed in Ref. 19, where the edge of graphene on nanopillar arrays were found to have anisotropic stretching strain due to structural asymmetries and force imbalances.

REFERENCES

1. Chua, L. L.; Zaumseil, J.; Chang, J. F.; Ou, E. C.; Ho, W. P. K. H.; Sirringhaus, H.; Friend, R. H. General Observation of N-Type Field-Effect Behaviour in Organic Semiconductors. *Nature* **2005**, 434, 194–199.
2. Suk, J. W.; Kitt, A.; Magnuson, C. W.; Hao, Y. F.; Ahmed, S.; An, J. H.; Swan, A. K.; Goldberg, B. B.; Ruoff, R. S. Transfer of CVD-Grown Monolayer Graphene onto Arbitrary Substrates. *ACS Nano* **2011**, 5, 6916−6924.
3. Das, A.; Pisana, S.; Chakraborty, B.; Piscanec, S.; Saha, S. K.; Waghmare, U. V.; Novoselov, K. S.; Krishnamurthy, H. R.; Geim, A. K.; Ferrari, A. C.; Sood, A. K. Monitoring Dopants by Raman Scattering in an Electrochemically Top-Gated Graphene Transistor. *Nat. Nanotechnol.* **2008**, 3, 210–215.
4. Lee, J. E.; Ahn, G.; Shim, J.; Lee, Y. S.; Ryu, S. Optical Separation of Mechanical Strain from Charge Doping in Graphene. *Nat. Commun.* **2012**, 3, 1024.
5. Neumann, C.; Reichardt, S.; Venezuela, P.; Drögeler, M.; Banszerus, L.; Schmitz, M.; Watanabe, K.; Taniguchi, T.; Mauri, F.; Beschoten, B.; Rotkin, S. V.; Stampfer, C. Raman Spectroscopy as Probe of Nanometre-Scale Strain Variations in Graphene. *Nat. Commun.* **2015**, 6, 8429.
6. Grason G. M.; Davidovitch, B. Universal Collapse of Stress and Wrinkle-to-Scar Transition in Spherically Confined Crystalline Sheets. *Proc. Natl. Acad. Sci. USA* **2013**, 110, 12893–

12898.
7. Zhou, Y.; Chen, Y.; Liu, B.; Wang, S.; Yang, Z.; Hu, M. Mechanics of Nanoscale Wrinkling of Graphene on a Non-Developable Surface. *Carbon* **2015**, 84, 263−271.
8. Yoon, D.; Son, Y.-W.; Cheong, H. Strain-Dependent Splitting of the Double-Resonance Raman Scattering Band in Graphene. *Phys. Rev. Lett.* **2011**, 106, 155502.
9. Mohiuddin, T. M. G.; Lombardo, A.; Nair, R. R.; Bonetti, A.; Savini, G.; Jalil, R.; Bonini, N.; Basko, D. M.; Galiotis, C.; Marzari, N.; Novoselov, K. S.; Geim, A. K.; Ferrari. A. C. Uniaxial Strain in Graphene by Raman Spectroscopy: G Peak Splitting, Grüneisen Parameters, and Sample Orientation. *Phys. Rev. B* **2009**, 79, 205433.
10. Plimpton S. Fast Parallel Algorithms for Short-Range Molecular Dynamics. *J. Comput. Phys*. **1995**, 117, 1–19.
11. Humphrey W.; Dalke A.; Schulten K. VMD: Visual Molecular Dynamics. *J. Mol. Graph*. **1996**, 14, 33–38.
12. Lindsay L.; Broido D. A. Optimized Tersoff and Brenner Empirical Potential Parameters for Lattice Dynamics and Phonon Thermal Transport in Carbon Nanotubes and Graphene. *Phys. Rev. B* **2010**, 81, 205441.
13. Ong, Z. Y.; Pop, E. Effect of Substrate Modes on Thermal Transport in Supported Graphene. *Phys. Rev. B* **2011**, 84, 075471.
14. Nosé, S. A Unified Formulation of the Constant Temperature Molecular Dynamics Methods. *J. Chem. Phys.* **1984**, 81, 511–519.
15. Hoover W. G. Canonical Dynamics: Equilibrium Phase-Space Distributions. *Phys. Rev. A* **1985**, 31, 1695–1697.
16. Yamamoto, M.; Pierre-Louis, O.; Huang, J.; Fuhrer, M.; Einstein, T.; Cullen, W. "The Princess and the Pea" at the Nanoscale: Wrinkling and Delamination of Graphene on Nanoparticles. *Phys. Rev. X* **2012**, 2, 041018.
17. Elinski, M. B.; Liu, Z.; Spear, J. C.; Batteas, J. D. 2D or not 2D? The Impact of Nanoscale Roughness and Substrate Interactions on the Tribological Properties of Graphene and MoS_2. *J. Phys. D: Appl. Phys.* **2017**, 50, 103003.
18. Spear, J. C.; Custer, J. P.; Batteas, J. D. The Influence of Nanoscale Roughness and Substrate Chemistry on the Frictional Properties of Single and Few Layer Graphene. *Nanoscale* **2015**, 22, 10021–10029.
19. Jiang, Y.; Mao, J.; Duan, J.; Lai, X.; Watanabe, K.; Taniguchi, T.; Andrei, E. Y. Visualizing Strain-Induced Pseudomagnetic Fields in Graphene through an hBN Magnifying Glass. *Nano Lett.* **2017**, 17, 2839–2843.